CCFE
CULHAM CENTRE FOR FUSION ENERGY

UK Atomic Energy Authority

UKAEA-CCFE-CP(20)114

K Flinders, R Bamber, H Lewtas, D Hancock, D Homfray, J Kamalu, T Barrett

Characterising the Impact of First Wall Armor Castellations on the Efficiency of Induction Heating During High Heat Flux Testing in the HIVE Facility

Characterising the Impact of First Wall Armor Castellations on the Efficiency of Induction Heating During High Heat Flux Testing in the HIVE Facility

K Flinders, R Bamber, H Lewtas, D Hancock, D Homfray, J Kamalu, T Barrett

This paper has been submitted to
30th Symposium on Fusion Technology (SOFT), Giardini Naxos, Messina, Sicily, 16-21 September 2018

Characterising the Impact of Castellations on the Efficiency of Induction Heating During Testing in the HIVE Facility

K Flinders[a], R Bamber[a], H Lewtas[a], D Hancock[a], D Homfray[a], J Kamalu[b], T Barrett[a]

[a] *Culham Centre for Fusion Energy, Culham Science Centre, UK*
[b] *University of the West of England, Bristol, UK*

High heat flux testing is a vital part of engineering component validation for fusion technology. The Heat by Induction to Verify Extremes (HIVE) facility is designed to provide a practical avenue for this aspect of component testing. It provides fast turnaround for smaller concepts and a cost-effective approach by utilising induction heating within a small vacuum vessel. Due to the potential complexity of induced current paths in an induction heating system, the extent and homogeneity of power coupled to a component is difficult to model. This uncertainty increases where components have geometrical features such as the grid pattern castellations that are often present on plasma facing components in fusion reactors. This project investigates the influence of various castellation patterns on the coupling characteristics of HIVE. It shows for example that as the grid density of castellations is increased, the applied heat flux increases from 4.5 MW/m2 to 6.85 MW/m2 for an input power of 30kW, due to an improvement in the efficiency of the inductive coupling from 13.4% to 20.6%. Additional experimental factors affecting efficiency and homogeneity of heating are also discussed.

Keywords: Induction, High Heat Flux, Castellations, HIVE, First Wall

1. Introduction

To ensure the success of both JET and ITER, comprehensive design and fusion relevant heat flux testing of the first wall components must be undertaken. One testing platform currently undergoing commissioning is the Heat by Induction to Verify Extremes (HIVE) facility at Culham Science Centre, UK[1]. This facility uses the principle of electromagnetic induction to apply a surface heat flux to prototype components and assemblies.

A common feature found on many first wall and divertor components is a 'castellated' or grid-cut front face, used to reduce secondary stresses and mechanical reaction to magnetic eddy currents. The effect that these castellations have on the induction heating process was, up to this point, untested. This experiment was required to prove the suitability of HIVE for the high heat flux testing of castellated prototypes. To represent the varying castellated patterns, five different samples were tested, each with its own grid pattern applied.

The aim of this experiment was to validate the use of the HIVE facility on castellated geometries and prototypes. Achieving this by demonstrating the impacts of such geometries on both the overall coupling efficiency of the induction system and the homogeneity of the heat distribution across the front surface of the five tungsten samples, during a range of heating cycles and configurations.

1.2 Induction Heating Considerations [2]

There are numerous electro-magnetic phenomena associated with the induction heating process, three of which were thought to influence the experiment in a significant way.

The 'Skin Effect' - For this application the skin depth in the experiment samples can be considered to be 0.4mm. This relatively shallow skin depth shows that the applied heat flux can be treated as a surface flux. See [3] for further information.

The 'Proximity Effect' – This explains the relationship between the distance from the primary conductor (induction coil) to the secondary conductor (the sample) and the current density/power density transferred between them. In relation to this experiment this sets the requirement for accurately setting the coil distance from the sample as it can have a significant impact on both the coupled power and the homogeneity of the heat distribution.

'End/Edge Effects' - Edge effects are described as a distortion in the electromagnetic field at the 'ends' or 'edges' of a conductor, that in turn affects the current density distribution by tending currents towards the edges of a component or workpiece [2]. When considered in relation to the castellated geometries this was thought to have a potential impact on both the homogeneity and the coupling efficiency, see Figure 1.

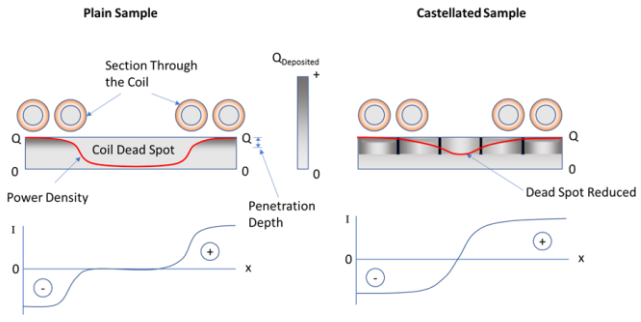

Figure 1 - Illustration of the End/Edge Effects & Coil 'Dead-Spot'

author's email: kieran.flinders@ukaea.uk

This would suggest the more castellated samples would have better coupling efficiency and homogeneity due to the increased number of edges. In turn leading to the formation of larger current densities within an increased proportion of the overall volume of the sample.

2. Method

This experiment comprised of three distinct stages:

1) Use of heat transfer methods to generate predictive simulations of the heat transfer through the samples. This information was used for the mount design and to outline an experimental heating program covering a sufficient range of inputs, see Section 2.2 for details.

2) Considering the information gained in the first stage, design and manufacture a suitable mount to hold the sample that allowed for high temperatures to be reached.

3) To assess both the inductive coupling efficiency and the homogeneity of heat transfer using a pattern of thermocouples and a visual camera.

2.1 Sample Description and Preparation

Before the experiment was started the samples were prepared by attaching 5 thermocouples in a specific and consistent pattern. The samples are illustrated in Figure 2 with the associated thermocouple pattern in Figure 3, chosen to ensure the important areas of the castellated geometry were monitored (bottom of the grooves, center of the grids etc).

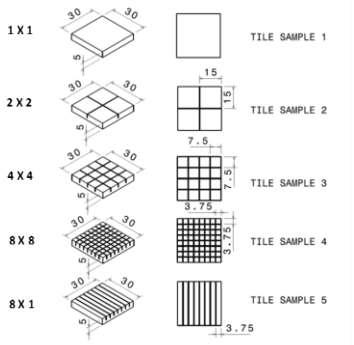

Figure 2 - The Five Tungsten Samples

K-Type thermocouples manufactured to the JET specification were used for the temperature monitoring, these were installed in an unsheathed, grounded configuration using a percussion welding technique. This created a permanent bond between the thermocouple and the sample. Figure 3 shows a representative image of the thermocouple installation alongside the employed pattern.

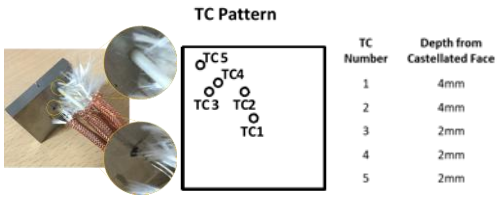

TC Number	Depth from Castellated Face
1	4mm
2	4mm
3	2mm
4	2mm
5	2mm

Figure 3 - Thermocouple Installation

A thermocouple was also attached to the surrounding metal frame-work of the mounting structure. This provided monitoring for thermal leakage into the structure and data for use in the results analysis, described in Section 3.

2.2 Heating Program

To develop a program based on the approximate heating of the sample during the experiments a numerical model was generated. Based on the heat balance equation for a lumped body, the main formula used for this simulation was,

$$\frac{dT}{dt} = \frac{Q_{in} - Q_{cond} - Q_{rad}}{mC_p} \quad (1)$$

which becomes,

$$\frac{dT}{dt} = \frac{Q_{in} - \left(\frac{1}{T_r}(T_s - T_{surr})\right) - \left(\varepsilon\sigma F A_s (T_s^4 - T_{surr}^4)\right)}{mC_p} \quad (2).$$

Due to the complex nature of predicting coupling efficiency for the HIVE induction system the value for Q_{in} was calculated over a range of predicted coupling efficiencies. This range was initially from 5% to 30% efficiency. The conductive and radiative losses Q_{cond} and Q_{rad} were approximated using a thermal resistance network and radiative principles respectively. The constant factors of each of these loss parameters were then treated as coefficients '*a*' for the conductive losses and '*b*' for the radiative losses.

The results for dT/dt from these calculations were then used to generate an approximate thermal map of the entire experimental cycle of heating and cooling phases (10 cycles in total). This ensured the chosen pulse characteristics did not breach the experimental limits (1250°C – the limit of K-type thermocouples) and that the experiment covered a sufficient temperature and power input range.

Upon completion of preliminary tests, using a representative tungsten sample, it was found that the initial experimental heating program, described above, was too conservative for the actual system coupling efficiency and cooling characteristics. The program was therefore updated to suit by reducing the cooling times and increasing the power cycle durations. This updated plan is show in Figure 4.

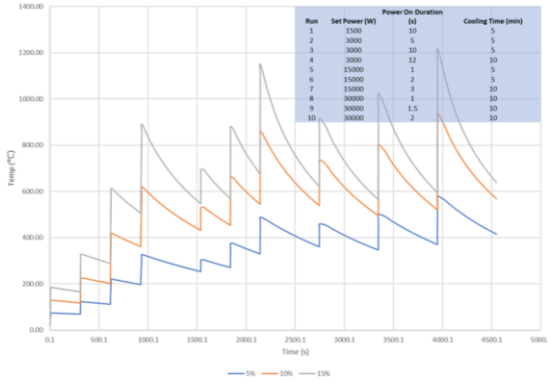

Figure 4 - The Final Experimental Program Showing Thermal Cycle Across 5, 10 & 15% Coupling Efficiency

2.3 Experimental Testing & Observation

The heating program was followed for each individual sample. To ensure that the coil distance from the sample remained consistent throughout, a feeler gauge was used to confirm positioning after every sample change. For each sample a thermal trace was recorded from each of the five thermocouples, however, due to thermocouple failure, all five thermocouples were not recorded on all samples. Alongside the thermocouple traces, a digital camera was used to record runs 7 and 10, where the sample reached sufficient temperature to glow in the visible spectrum. This data was used to gain an idea of the homogeneity of the induction heating. Still frames showing this are pictured in Figure 5, where the coil 'dead-spot' (see Figure 1) can be seen. This is discussed further in Section 4.

Figure 5 - Still Frames Showing Heat Distribution

3. Power & Efficiency Calculations

The data analysis was set up in a similar way to the numerical model. However, for this experimental temperature data was used to determine coupled power and efficiency, rather than the set power and efficiency to determine temperature. There were two differences between this and the original model, the first is that the emissivity value was changed to become temperature dependent. The second is within the calculations for conductive losses, where rather than using a fixed value of 25°C for the ambient temperature (T∞), the frame thermocouple was used to provide a real experimental value for this factor. Therefore improving the initial accuracy of the power calculations.

To analyse the results for the determination of gross coupling efficiency for each sample, the experimental thermocouple traces were averaged and broken down into power in and cooling phases for each pulse. This provided the ability to fit the heat loss coefficients, '*a*' and '*b*' from the numerical model, against the experimental cooling curve. The resultant values for the coefficients were then applied to the calculations for gross power input.. This was the first stage of the analysis process and was completed for each 'pulse' for all samples.

After the fitted loss coefficients had been obtained, the next stage was to determine the gross coupled power into the sample, using a heat balance for a 0.1 second timestep. Where gross power accounts for both conductive and radiative thermal losses from the sample. Finally, an average power was then obtained for the entire pulse.

The value from this calculation was then translated into a value for overall efficiency covering the complete heat in cycle, using Equation 3,

$$Efficiency\ in\ \% = \frac{Q_{Gross}}{P_{Set}} X\ 100 \qquad (3).$$

These calculations were performed for each pulse on each sample. Table 1 is the summary table for sample 4.

Table 1 - Sample 4 Summary Table

		Set Power	Duration	Gross Coupled Power	Overall Efficiency	Applied Heat Flux	Max Temp	Ave Temp
		(kW)	(s)	(W)	(%)	(MW/m^2)	(°C)	(°C)
PULSE NO.	**1**	1.5	10	71	**4.7**	0.08	84.9	**57.9**
	2	3	5	249	**8.3**	0.28	163.2	**118.2**
	3	3	10	268	**8.9**	0.30	319.9	**226.5**
	4	3	12	328	**10.9**	0.36	473.7	**358.5**
	5	15	1	2574	**17.2**	2.86	419.8	**334.4**
	6	15	2	2831	**18.9**	3.15	651.8	**476.7**
	7	15	3	3267	**21.8**	3.63	911.1	**655.9**
	8	30	1	6320	**21.1**	7.02	687.0	**497.2**
	9	30	1.5	6540	**21.8**	7.27	835.4	**559.9**
	10	30	2	6233	**20.8**	6.93	1012.2	**656.2**

4. Results

When looking at the samples individually, such as in Table 1 for sample 1, there are two relationships that can be identified, the first is that the efficiency appears to increase as the temperature is increased, and the second is that as the set power is increased, again the overall coupling efficiency appears to rise alongside it, these observations are discussed in more detail in Section 4.2. The average efficiency from each sample type was calculated across the entire experimental run, these results were then compared across all five samples to produce a summary table for the entire experiment, see Table 2.

Table 2 - Summary Table for All Samples

		Set Power In	Duration	Sample Overall Efficiency						
				Sample 1 (1x1)	Sample 1 (rpt)	Sample 2 (2x2)	Sample 2 (rpt)	Sample 3 (4x4)	Sample 4 (8x8)	Sample 5 (8x1)
		(kW)	(s)	(%)	(%)	(%)	(%)	(%)	(%)	(%)
PULSE NO.	**1**	1.5	10	**2.5**	**2.8**	**3.0**	**3.4**	**3.5**	**4.7**	**3.2**
	2	3	5	**4.2**	**4.6**	**5.2**	**5.5**	**6.3**	**8.3**	**5.7**
	3	3	10	**4.6**	**5.0**	**5.8**	**5.8**	**6.9**	**8.9**	**6.2**
	4	3	12	**5.2**	**5.8**	**6.8**	**7.0**	**8.1**	**10.8**	**7.3**
	5	15	1	**8.6**	**10.0**	**12.1**	**12.6**	**14.2**	**17.2**	**12.6**
	6	15	2	**10.4**	**10.6**	**13.3**	**13.6**	**14.8**	**18.9**	**13.9**
	7	15	3	**12.4**	**12.4**	**15.1**	**14.8**	**15.9**	**20.6**	**14.9**
	8	30	1	**12.4**	**12.4**	**15.0**	**15.6**	**16.5**	**20.4**	**15.8**
	9	30	1.5 (**2**)	**12.8**	**13.4**	**14.8**	**15.2**	**17.1**	**20.8**	**15.1**
	10	30	2 (**3**)	**13.4**	**14.7**	**15.8**	**16.0**	**17.2**	**20.6**	**16.6**
			Average Efficiency	**8.7**	**9.2**	**10.7**	**11.0**	**12.1**	**15.1**	**11.1**

4.1 Coupling Efficiency

Table 2 shows that the coupling efficiency improves with the number of castellations. This agrees with the electromagnetic edge effect theory as the increased geometrical 'edges' also increase the distributed current across the sample. However, there is also an increase in the coupling efficiency as a function of temperature across all samples, this is examined in more detail in Section 4.2

To show the relationship between the castellated geometry and the coupling efficiency, the area of each grid square of the castellated pattern for each sample is plotted against the overall coupling efficiency for each sample, see Figure 6 where the efficiency of the inductive coupling is shown to increase as the castellation area decreases.

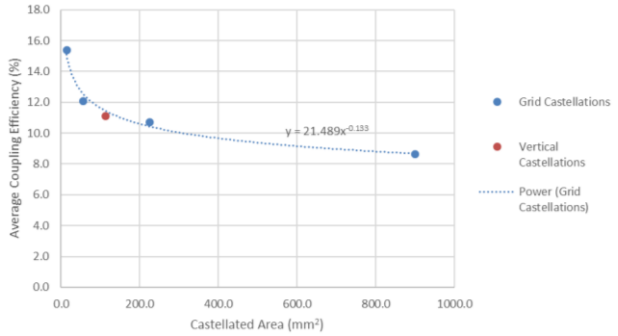

Figure 6 – Av. Coupling Efficiency Against Castellation Area

This relationship displays an overall comparison between the density of the castellated grid and the efficiency of coupling. Thereby proving that castellated components do indeed influence the inductive coupling efficiency. It is thought that this is caused by the increase of geometrical 'edges', which in turn increase the overall current density across the face of the tile, due to the inductive 'edge' effects.

The above also holds when looking at the comparison between castellation size and efficiency for specific pulses, Figure 7 shows an example of pulse 4 (3kW for 12s) and pulse 7 (15kW for 3s), where a similar relationship can be seen linking castellation size and efficiency.

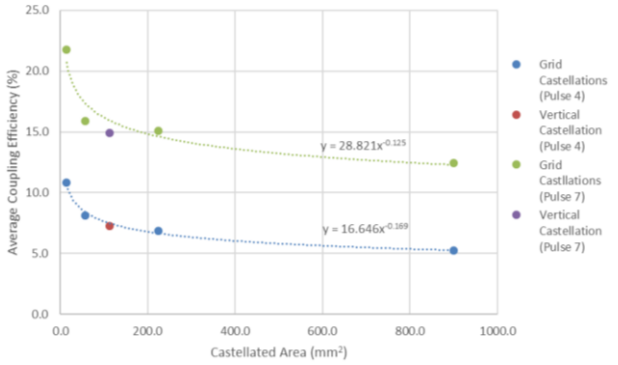

Figure 7 - Coupling Efficiency Against Castellation Area for 3kW and 15kW

4.2 Temperature and Power

As seen in Figure 7, there is a large difference in coupling efficiency between the 3kW and 15kW power settings. The main factor affected by temperature is the resistivity of the material. This has an impact on both the magnitude of the applied power, through the 'Joule Effect', and the current distribution, through the penetration depth principle explained by the 'skin effect'. When comparing the normalised resistivity and penetration depth trends for tungsten against temperature, a linear trend can be seen in both. Combined additively, this increase is directly proportional to the average temperature vs efficiency during low power pulses, explaining this increase.

4.3 Homogeneity

Through the videos and their associated still images a qualitative idea of the homogeneity of the thermal coupling can be obtained. It can be seen that thermal transfer starts from the edges of the sample, as predicted by the thermal edge effects explained in Section 1.

As the number of castellations increased, the 'dead spot' seemed to reduce and the heating appeared more uniform. There was also a slight bias towards the top right-hand corner of the tile, caused by either coil design or positioning. As with the coupling efficiency there was less pronounced difference between the 2x2 and 4x4 grid castellated and non-castellated samples when comparing the apparent heating uniformity. The presence of the coil 'dead spot' does seem to reduce on the more castellated samples, again, likely due to the increased current density at the castellated edges as shown in Figure 1.

5. Conclusions

During the heating cycle, much of the current is transmitted into the edges of the components, this is therefore where most of the heating takes place, shown in the visual images of the tile heating process.

The homogeneity appears to differ slightly between different levels of castellations, with a slight decrease in the coil dead spot. Overall the castellated geometry has much less of an effect on the homogeneity of the heating than the coupling efficiency. Further research into coil design is likely to improve this aspect.

The coupling efficiency increases with the reduction in size of the castellated grid squares (and therefore the increasing density of the castellated grid). The non-grid style castellated component also fits the general trend. This increase is due to the thermal edge effects present during induction heating and the efficiency is related to the castellation size, approximately to the power of -0.133.

As well as the increase due to the castellations, the coupling efficiency also increases with temperature, with the resistivity of the material and the penetration depth of the inductive coupling as the cause.

HIVE may be effectively used for the high heat flux testing of castellated components from a coupling efficiency standpoint, considering each of the factors explained throughout this article. More research into coil design is required to improve homogeneity and thermal distribution across surfaces and further investigative work needed to quantify it using the thermal data.

References

[1] D. Hancock, Testing Advanced Divertor Concepts for Fusion Power Plants Using a Small High Heat Flux Facility, (2018).

[2] V. Rudnev, D. Loveless, R.L. Cook, Handbook of Induction Heating, 2nd ed., CRC Press, New York, 2017.

[3] K.Flinders, Inductive High Heat Flux Testing of Castellated Components, ERS/R/006, 2018.

This work has been carried out within the framework of the EUROfusion Consortium and has received funding from the Euratom research and training programme 2014-2018 under grant agreement No 633053. The views and opinions expressed herein do not necessarily reflect those of the European Commission.